International Journal of Heat and Fluid Flow 30 (2009) 158–171

Contents lists available at ScienceDirect

International Journal of Heat and Fluid Flow

journal homepage: www.elsevier.com/locate/ijhff

An experimental analysis of the flow pattern in heat exchangers with an egg carton configuration (parallel, convergent and divergent cases)

B. Girón-Palomares [a], A. Hernández-Guerrero [a,*], R. Romero-Méndez [b,1], F. Oviedo-Tolentino [b]

[a] Facultad de Ingeniería, Universidad de Guanajuato, Tampico 912, Salamanca, Guanajuato, 36730, Mexico
[b] Facultad de Ingeniería, Universidad Autónoma de San Luis Potosí, Av. Dr. Manuel Nava 8, Zona Universitaria, San Luis Potosí, SLP 78290, Mexico

ARTICLE INFO

Article history:
Received 31 December 2007
Received in revised form 15 September 2008
Accepted 21 September 2008
Available online 30 November 2008

Keywords:
Egg carton channel
Phase angle
Convergence/divergence angle
Unsteady flow
Steady flow
Recirculation
Significant-mixing

ABSTRACT

An experimental analysis about the flow patterns that appear in the channel formed between two corrugated plates with an egg carton configuration is reported. The types of flow instabilities caused by the corrugated plates are identified and described by means of flow visualization experiments, and photographic sequences illustrate the flow features present for each case. The influence on flow instabilities of Reynolds number, phase angle, convergence/divergence angle and spacing between corrugated plates is investigated. The corrugated plates are set divergent and convergent in order to investigate if recirculations are broken by chaotic advection. The improvement of heat transfer in the laminar regime has become an essential task in many applications and therefore the experiments are conducted in this regime.

The corrugated plates geometry provides two main advantages over the conventional plane plates: the recirculation zones observed in the longitudinal direction and the three-dimensionality of the flow, i.e. the recirculations reduce the thermal resistances while the three-dimensionality of flow generates a better mixing and a more uniform temperature distribution.

This experimental study contributes to the general knowledge on the subject being the first that addresses the analysis of convergent and divergent egg carton plates. It is expected that the results presented here will shed some light as to advantageously use these geometries in the near-future heat exchangers. (Because of the improve chaotic mixing in divergent corrugated plates, this configuration may be a good option to improve heat exchangers performance, because a better mixing is always related to the presence of core fluid near exchange surfaces, and consequently an increase in temperature gradients and heat transfer.)

1. Introduction

Obtaining good fluid mixing, reduction of heat transfer resistances, and minimum pressure drops are very important factors in the design of heat transfer devices. Good mixing may be obtained by operating heat exchangers in the turbulent regime, although the turbulent regime implies high pressure drop. Operating heat exchangers in the turbulent regime increases the pumping costs, which is a limiting factor in some applications, such as compact heat exchangers and heat transfer of high viscosity fluids. Additionally, in recent times, heat transfer under laminar flow conditions has assumed relevance in applications such as bioreactors and blood oxygenators (Nishimura and Kawamura, 1995).

Several techniques have been used to enhance heat transfer in plate heat exchangers (Braun et al., 1999; Herman and Kang, 2002; Lyman et al., 2002), one of the most frequent one uses wavy plates instead of flat plates. Many investigations (most of them numerical) have demonstrated that using sinusoidal plates instead of flat plates improves the heat transfer without a large increase in pressure drop (Gschwind et al., 1995; Islamoglu and Parmaksizoglu, 2004; Jang and Chen, 1997; Mahmud et al., 2002; Rush et al., 1999; Sawyers et al., 1998; Wang and Chen, 2002; Zhang et al., 2004).

Some researchers have proposed to improve laminar mixing in those applications by means of chaotic advection. When the fluid presents pathlines that do not conform to the laminar regime, such fluid presents chaotic advection. Chaotic particle paths can be found in two-dimensional time-depending flows as well as in three-dimensional flows. There are two ways to promote chaotic mixing in two-dimensional systems with deterministic particle paths. One of those techniques consists of perturbing the flow by means of an external periodic force that creates transient flow, the other one consist of generating a three-dimensional flow component. Chaotic mixing can be generated in ducts, if the duct geometry is periodically perturbed in the downstream direction. Clear examples of how to improve heat transfer by means of

* Corresponding author. Tel.: +52 464 64 79940x2382.
E-mail addresses: abelh@salamanca.ugto.mx (A. Hernández-Guerrero), rromerom@uaslp.mx (R. Romero-Méndez).
[1] Tel.: +52 444 817 33 81.

0142-727X/$ - see front matter © 2008 Elsevier Inc. All rights reserved.
doi:10.1016/j.ijheatfluidflow.2008.09.005

Nomenclature

A	dimensional amplitude, cm
h	distance between upper wall and channel centerline, cm
H_{avg}	average channel width, cm
V_{in}	average inlet channel velocity, cm s^{-1}
Re	Reynolds number, dimensionless
x, y, z	cartesian coordinate system

Greek symbols

α	convergence/divergence angle
ϕ	phase angle
β	dimensionless amplitude
λ	dimensionless wavelength
Λ	dimensional wavelength, cm
ν	kinematic viscosity, cm^2 s^{-1}

Subscripts

x, z	x and z directions

chaotic advection are available in the literature (Chagny et al., 2000; Chang and Sen, 1994; Froncioni et al., 1997; Galaktionov et al., 2002; Howes and Shardlow, 1997; Jones, 1994; Lefevre et al., 2003; Lemenand and Peerhossaini, 2002; Liu et al., 1994; Mokrani et al., 1997; Raynal and Gence, 1997; Sawyers et al., 1998; Southerland etal., 1994; Tabor and Klapper, 1994). As an example, Mokrani et al. (1997) experimentally investigated chaotic advection as a means to improve heat exchanger performance. They compared the behavior of two shell-and-tube heat exchangers: a helical-coil heat exchanger and a twisted pipe-coil heat exchanger (chaotic heat exchanger). The chaotic heat exchanger was assembled with bends and straight tubes. The bends were set in such a way that neighboring bends were orthogonal in order to generate three-dimensional flow as well as chaotic behavior. These authors performed experiments for Reynolds numbers between 60 and 200. They demonstrated that the temperature profile of the chaotic heat exchanger is better distributed than that of the helical-coil heat exchanger. This behavior is caused by the chaotic particle paths that improve the mixing in the chaotic heat exchanger. Finally, these authors determined that the relative enhancement in performance of the chaotic heat exchanger, in comparison with the helical-coil heat exchanger, was of the order of 13–28%.

Another clear example that shows how to generate chaotic advection is the research performed by Liu et al. (1994). They studied mixing characteristics in chaotic periodic flows as well as in chaotic non-periodic flows, numerically determining the position of particles in a two-dimensional rectangular cavity with two moving walls. They induced transient flow and chaotic paths by displacing periodically or aperiodically the moving walls, finding that the mixing distribution in aperiodic flows is better than in periodic flows (thus the heat transfer is better in aperiodic flows).

On the other hand, some non-conventional ways have been introduced to enhance the behavior in plate heat exchangers, and one of the most important ones is wavy plates instead of flat plates. The fluid convective thermal resistance is reduced by means of this technique. Some investigations have demonstrated that using sinusoidal plates instead of flat plates improves the heat transfer without a great increase in the pressure drop (Gschwind et al., 1995; Islamoglu and Parmaksizoglu, 2004; Jang and Chen, 1997; Mahmud et al., 2002; Rush et al., 1999; Wang and Chen, 2002; Zhang et al., 2004).

Recently, the flow pattern in plates with corrugations in the transversal and parallel directions to the flow (*egg carton configuration*) has been investigated by means of an analytic-numerical technique (Sawyers et al., 1998). This kind of investigation is one of the most innovative in relation to corrugated plates as a means to improve the heat transfer, and it could provide state of the art knowledge about the existence of chaotic particle paths in egg carton channels. Sawyers et al. (1998) investigated the flow pattern between two corrugated plates with the egg carton configuration and a 180° phase angle. They determined the flow characteristics in steady state, paying special attention to the way to improve the heat transfer by generating chaotic particle paths in three-dimensional steady flows. For zero angle of attack, in symmetry planes, it was determined that the flow pattern is similar to the flow pattern in sinusoidal corrugated plates. For small flow angles ($0° < \alpha \leqslant 2.37°$), particles leave recirculation zones, and incorporate to the main core flow, allowing an enhancement in the heat transfer, compared to recirculation zones in flows with zero angle of attack. When the angle of attack is large ($\alpha > 2.37$), the recirculation region is destroyed by the transverse flow, and the heat transfer diminishes.

Steady state is assumed in most of the analytical and numerical investigations in relation to corrugated sinusoidal plates, however, some experimental evidence (Stone and Vanka, 1999) has demonstrated that steady state is only reached for very small Reynolds numbers. As the Reynolds number is increased, the flow close to the corrugated plate channel outlet becomes unsteady, and the instabilities approach the corrugated plate channel inlet. At very high Reynolds numbers, instabilities appear in the entire channel with the exception of the first wave (not at the channel inlet, but downstream from it), which shows steady state at very high Reynolds numbers. Sawyers et al. (1998) considered steady flow in their investigation of flow in egg carton channels.

The present experimental investigation studies the flow pattern in corrugated plates with the egg carton configuration. The types of instabilities as well as their relationship to the Reynolds number, the phase angle, convergence/divergence angle, and the spacing between corrugated plates is studied. Additionally, it is investigated if recirculation zones are broken by chaotic advection when the corrugated plates are set divergent or convergent. Apart from this study being an experimental one, which in itself contributes to the general knowledge on the subject, another important novelty is to include the analysis for convergent and for divergent egg carton plates, which has not been yet reported in the technical literature has undertaken. It is expected that the results presented here will shed some light as to advantageously use these geometries in the design of future heat exchangers.

2. Experimental methodology

Experimental flow visualization methods have been used in order to investigate the flow pattern in a wide array of very important problems in fluid mechanics (DeJong and Jacobi, 2003; El-Sayed et al., 2002; Lin et al., 2002; Romero-Méndez et al., 2000; Rush et al., 1999). For example, Rush et al. (1999) successfully used flow visualization by injecting dye to establish the flow pattern characteristics that exist between two finite sinusoidal corrugated plates. The flow visualization methods that use water as the working fluid are very appropriate for visualizing the flow pattern between two corrugated plates in plate heat exchangers. Using water as the working fluid enables one to establish appropriate

spacing between plates and adequate fluid velocities for good visualization.

This investigation uses the seeding of reflective micrometric particles in water in order to visualize the flow. These particles are hollow glass spheres coated with silver to allow the best light reflection; in addition to this advantage, the particles are small enough to approximately follow the fluid particle paths. The particle paths in the plane under study were illuminated by a light sheet created by a light source. The micrometric particle paths are recorded by means of photographs taken with a camera set up so that its vision line is perpendicular to the visualization plane.

The experiments were performed in a water tunnel with a test section 0.381 m wide, 0.508 m high and 1.5 m long (see Figs. 1–6). The walls and bottom of the test section are made of tempered glass for visual access to the model being tested. The water tunnel may be operated at velocities ranging from 0.01 to 0.3 m/s. The downstream end of the delivery plenum of the water tunnel has a section with flow conditioning elements. The first is a perforated stainless steel plate, which reduces the turbulence level. The last is a honeycomb flow straightener. The contraction section of the water tunnel has an area ratio of 6:1. This geometry provides good velocity distribution and avoids local separation and vorticity development.

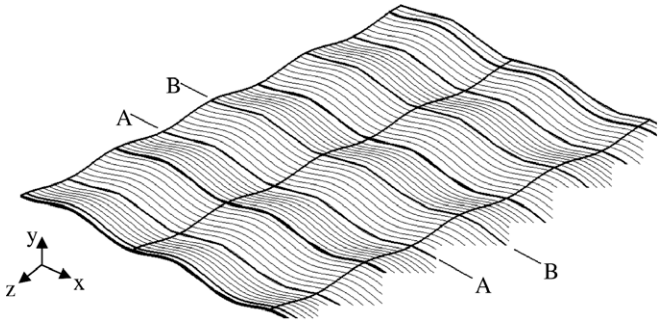

Fig. 1. Portion of one corrugated plate with the egg carton configuration.

The visualization particles are illuminated with the light emitted from a 30 mW He–Ne laser lamp, which has been opened into a light sheet by a cylindrical lens. The laser light was cast through the bottom of the water tunnel to illuminate a fan-shaped plane, that serves to keep track of the two-dimensional motion of seeded particles on a vertical plane inside the experimental model. The room where the experiments took place was completely darkened in order to avoid the presence of any light source other than the laser light sheet.

A reflex photographic camera with a 50 mm f/2.5 compact macro lens, and a black and white photographic film was used to capture the streaks traced by the suspended particles. Exposure times were chosen depending on the flow velocity, and the values used were 0.7, 1, 1.5 and 2 s, with diaphragm adjustments of 4.5, 5.6 and 6.7, respectively. Extended developing times were used in order to sensitize the negative to the presence of very dim light. The images presented in this paper were digitized after printing the photographs taken during the experiments.

Fig. 1 shows the geometric configuration of one of the plates with egg carton configuration used to form the channel. The equation for the surface of the plates is

$$h = A_x \sin\left(\frac{2\pi x}{\Lambda_x}\right) + A_z \sin\left(\frac{2\pi z}{\Lambda_z}\right) \tag{1}$$

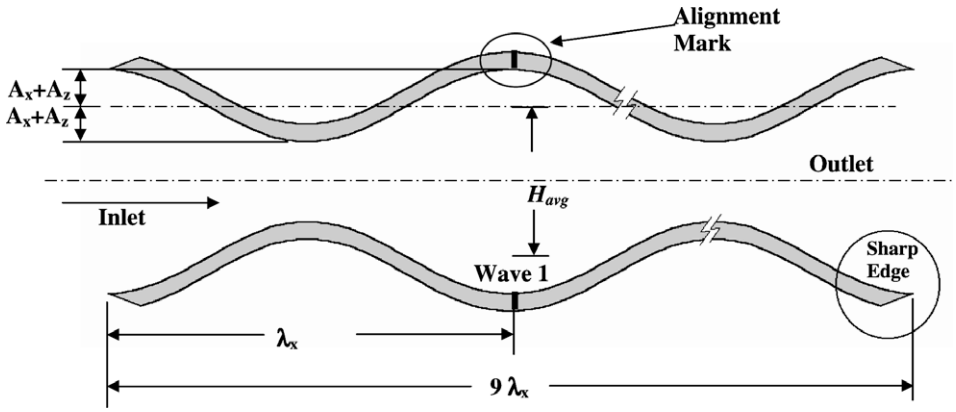

Fig. 2. Model A: 180° phase angle.

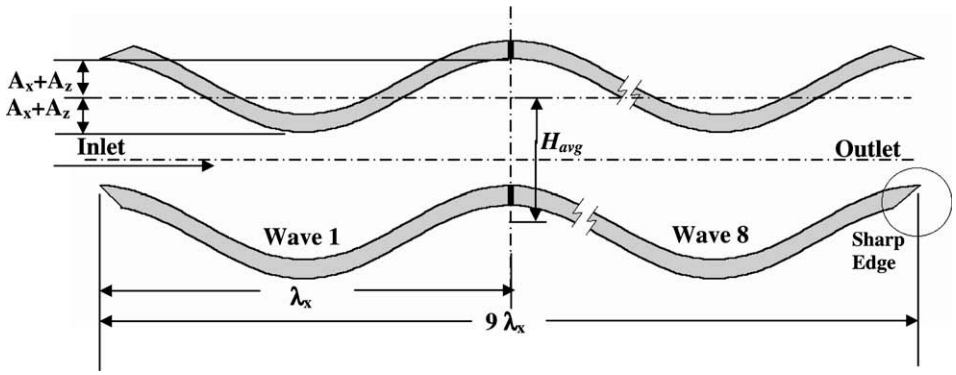

Fig. 3. Model B: 0° phase angle.

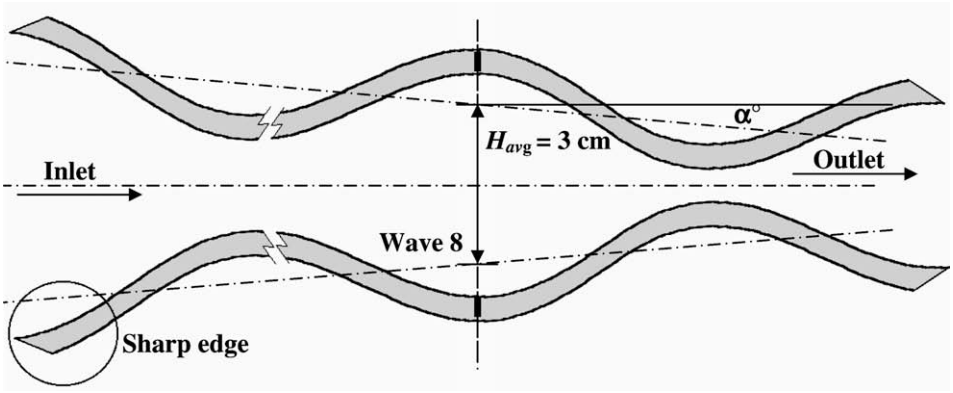

Fig. 4. Model 1: convergent corrugated plates.

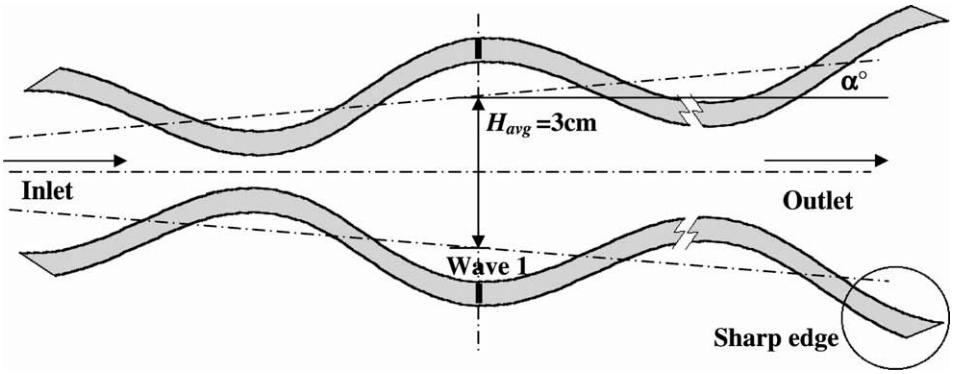

Fig. 5. Model 2: divergent corrugated plates.

where h is the height of the plate surface at a given coordinate x, z, with respect to the midplane, A_x and A_z are the wave amplitudes in the x and z directions, respectively, Λ_x, and Λ_z are the wavelengths in the x and z directions, respectively. The dimensions of the corrugated plates used in the experiments are: $A_x = 0.45$ cm, $A_z = 0.3$ cm, $\Lambda_x = 8.334$ cm, and $\Lambda_z = 7.625$ cm. The dimensions were defined in such a way that the dimensionless parameters used here were similar to those used in some investigations available in the literature (Rush et al., 1999 and Sawyers et al., 1998).

The dimensionless geometric parameters that describe the corrugated plate model with egg carton configuration, are the following: $\beta_x = A_x/H_{avg}$, $\beta_z = A_z/H_{avg}$, $\lambda_x = \Lambda_x/H_{avg}$, and $\lambda_z = \Lambda_z/H_{avg}$. H_{avg} is the separation between corrugated plates that form the channel (described with the aid of Fig. 2), which was fixed at $H_{avg} = 3$ cm throughout the investigation. The dimensionless values used here, in agreement with previous investigations, are $\beta_x = 0.15$, $\beta_z = 0.10$, $\lambda_x = 2.77$ and $\lambda_z = 2.54$.

Having established the dimensions of the model, the corrugated plates were built using a 2 mm thick Plexiglas plate (this thickness proved to satisfactorily support the flow loads). The Plexiglas optical properties allow the laser sheet to get through the plate without significant optical distortions. The corrugated plates were built by thermo-forming with male–female compression. The corrugated plates included nine corrugations in the x-direction and four corrugations in the *z-direction,* respectively.

The experimental models were divided in four models. For models A and B the plates were kept parallel with 180° and 0° phase angles, respectively. In model 1 the plates were set convergent, while the plates in model 2 were divergent. Figs. 2–5 show the experimental models as well as the definition of the average separation between plates.

Fig. 6 shows the experimental setup. The flow direction, the laser lamp and photographic camera positions, and the visualization planes can be observed. The laser lamp was set up so that the laser sheet produced was parallel to the principal flow and perpendicular to the corrugated plates. The visualization planes are planes with flow symmetry in order to observe clearly the recirculation zones and vortices present in the channel. The photographic camera was set so that its vision line was perpendicular to the visualization plane B. When plane A was visualized, the camera was set with a little inclination in order to visualize fully the wave over the bottom corrugated plate. In plane A was impossible to visualize both the waves in the bottom and top corrugated plates at the same time because the corrugations in plane A obstruct the view of the corrugations of plane B.

The Reynolds number was defined as

$$Re = \frac{V_{in} H_{avg}}{\nu} \tag{2}$$

where V_{in} is the average velocity at the inlet of the corrugated plates and ν is the fluid kinematic viscosity.

The Reynolds number was varied within the laminar regime (as observed from the flow visualization). For models A and B, the average separation between plates was varied from 3 to 5 cm. The average separation between plates was fixed to 3 cm in last wave of model 1 and in first wave of model 2 (see Figs. 4 and 5), this in order to compare with models A and B. Additionally, the convergence and divergence angles were varied in order to investigate their effect on the flow behavior. Some graphs and photographs that describe the flow behavior in each model are shown in the following section.

3. Results and analysis

In this section, important details of the flow pattern are illustrated and explained by means of photographs. The main flow

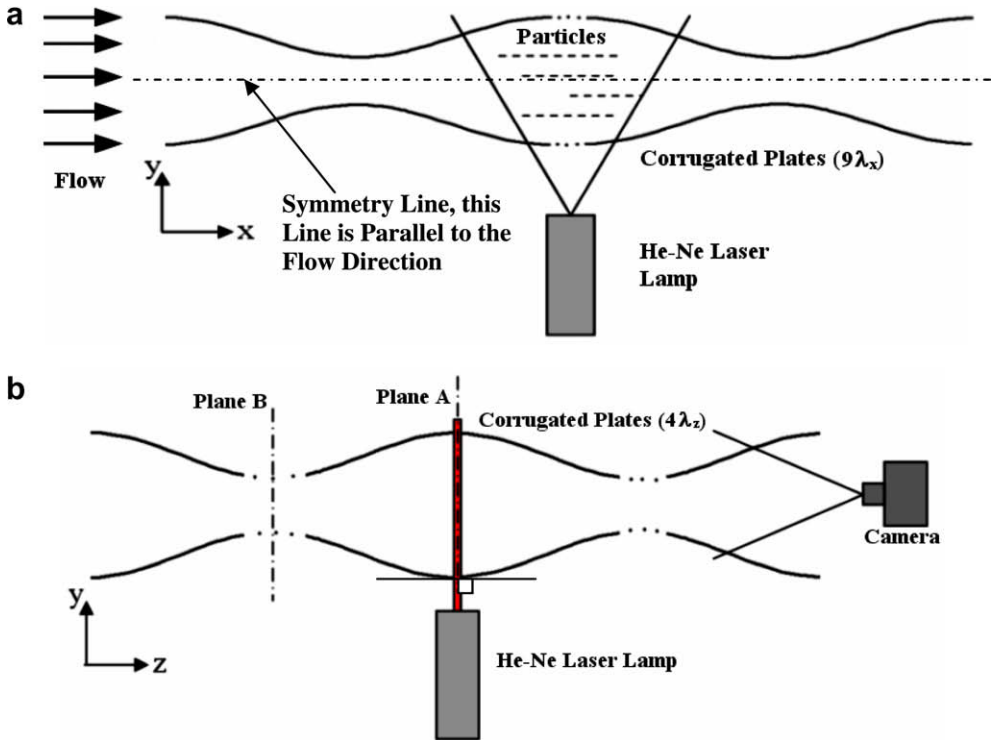

Fig. 6. Experimental setup. (a) View from a vertical and parallel plane to the main flow plane. (b) View from a vertical and perpendicular plane to the main flow (the main flow direction is perpendicular to this sheet).

direction in the photographs is from left to right. Additionally, the ranges of appearance of the different flow features are graphically represented.

3.1. Model A: 180° phase angle

The criterion used to determine if one wave has macroscopic mixing is the presence of crossing paths in the central flow, broken recirculation regions or too big rolling vortices compared to wave amplitude.

In Figs. 7–13 the results for this case are presented. Additional images were taken for the different *Re* numbers used, and the results are summarized in Figs. 8–13. For these experiments, the low Reynolds number limit was set at 200, while the upper limit was that in which mixing or random particle paths over the whole channel width were observed in waves 2 or 3. This kind of mixing or random particle path was called macroscopic mixing by Rush et al. (1999), and it will be called so in this work.

The flow pattern is very much like the one reported in previous investigations (Rush et al., 1999 and Wang and Chen, 2002). At small Reynolds numbers there are steady recirculation regions along the corrugated channel (see Fig. 7, wave 1). These recirculation regions have characteristics that are similar to those found in sinusoidal corrugated plates with 180° phase angle. The recirculation characteristics vary as the Reynolds number increases. When the Reynolds number increases, the separation point is closer to the inlet wave, and the reattachment point is closer to the outlet wave. The steady recirculation regions at the top and bottom corrugated plates are symmetrical with respect to the midplane of the channel. This can be observed in photographs of plane B shown in Fig. 7, wave 1.

For waves further from inlet flow instabilities appear in the channel. As the Reynolds number increases, instabilities appear in waves closer to the channel inlet. At very high Reynolds numbers (for this type of channels, it is known that at *Re* numbers of the order of 600 the flow shows already some instability), some waves present random particle paths that promote macroscopic mixing over all the separation between plates (see Fig. 7, wave 5). According to the observations, it was determined that the position of the first wave (number of wave counted from the channel inlet) with macroscopic mixing decreases as Reynolds number increases. However, macroscopic mixing was rarely observed in waves number 1 and 2, see Figs. 8–13. Graphs showing the macroscopic mixing behavior for each plane are included in this work (Figs. 8 and 9).

Having analyzed the flow pattern very carefully, other types of instabilities were observed at the high-end of the Reynolds number range studied. These instabilities are rolling vortices that appear in the limits between the principal flow and the upper part of the recirculation. The vortices appear in the wave inlet and move downstream to the wave outlet, where they join the principal flow. As the flow moves to the channel outlet, the vortices grow; for example, if one vortex is observed in wave 4, another vortex bigger and closer to the corrugated surface will be observed in wave 5. The rolling vortices replace the recirculation at high-end Reynolds numbers (see Fig. 7, wave 3). If rolling vortices appear in some wave of the channel, downstream from this wave, steady recirculation regions will not be observed and macroscopic mixing might appear. At a given Reynolds number, waves with rolling vortices and without macroscopic mixing may appear, however, a wave with macroscopic mixing never appears if there are not waves upstream with rolling vortices. According to this, it is believed that the macroscopic mixing is caused by instabilities in the central core flow that are created by rolling vortices upstream from the wave with macroscopic mixing. Finally, it is important to mention that rolling vortices and macroscopic mixing move closer to the channel inlet as the Reynolds number increases.

In general, the flow behavior observed in plane B is like that seen in plane A, but the values of Reynolds at which the flow features appear is different. Figs. 8–13 are graphs for the wave num-

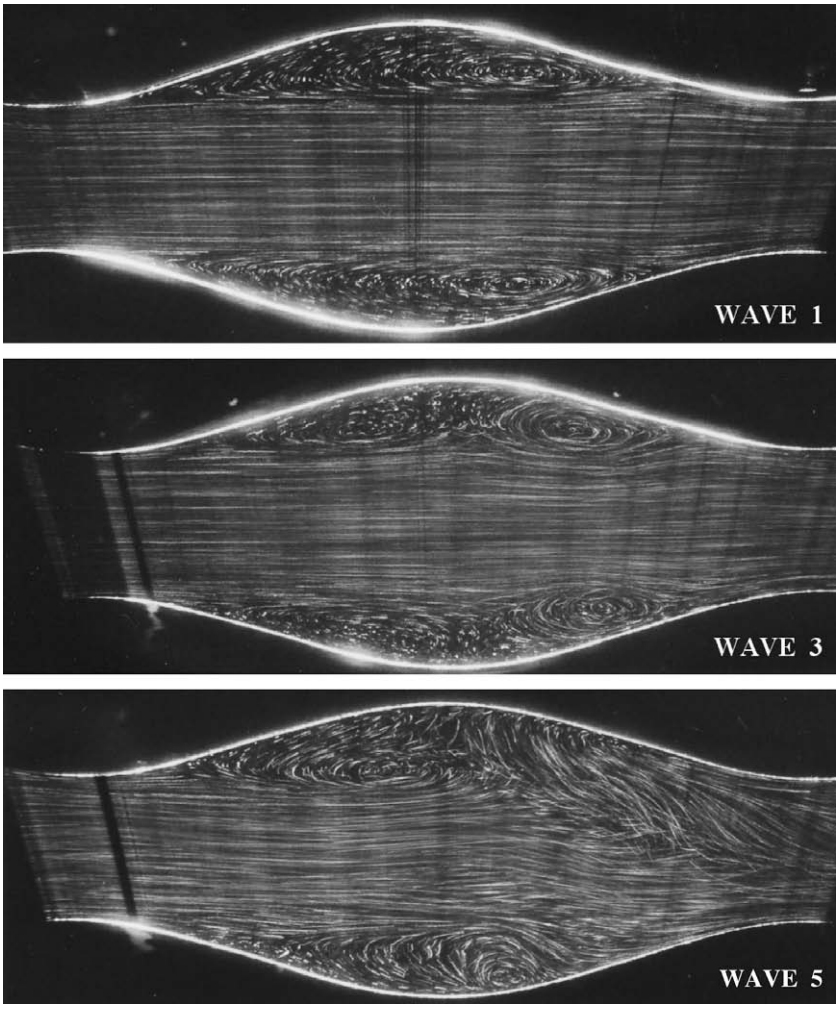

Fig. 7. Pathlines in the plane B, model A. H_{avg} = 3.0 cm, Re = 600.

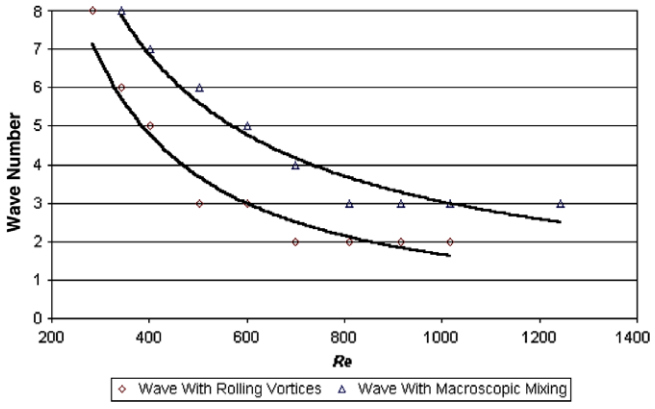

Fig. 8. Comparison between the position of the first wave that presents rolling vortices and the position of the first wave that presents macroscopic mixing. Model A, plane A, H_{avg} = 3.0 cm.

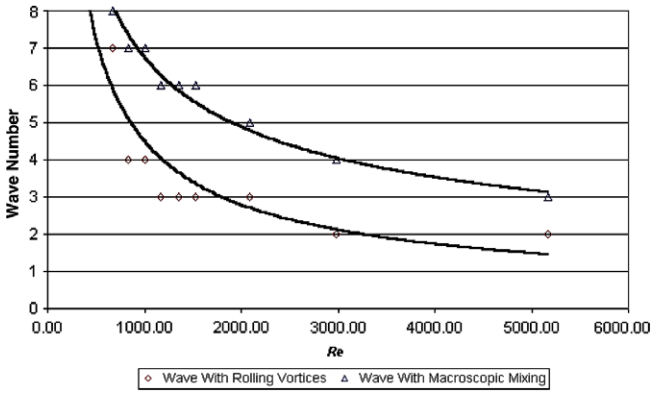

Fig. 9. Comparison between the position of the first wave that presents rolling vortices and the position of the first wave that presents macroscopic mixing. Model A, plane B. H_{avg} = 5.0 cm.

ber from inlet at which rolling vortices or macroscopic mixing appears.

When macroscopic mixing appears in some wave, there are waves upstream that have rolling vortices. This behavior is evident in Figs. 8 and 9. In addition to this behavior, it can be inferred that rolling vortex instabilities appear at lower Reynolds numbers than macroscopic mixing. This behavior is independent of the value of H_{avg} and is very similar in both planes of vision A and B.

Figs. 10 and 11 show the closest wave number from the inlet at which rolling vortices are visible for three different values of H_{avg}. The closest wave number to the inlet that presents macroscopic mixing can be observed in Figs. 12 and 13. In this figures the dashed lines represent the tendency of the pattern.

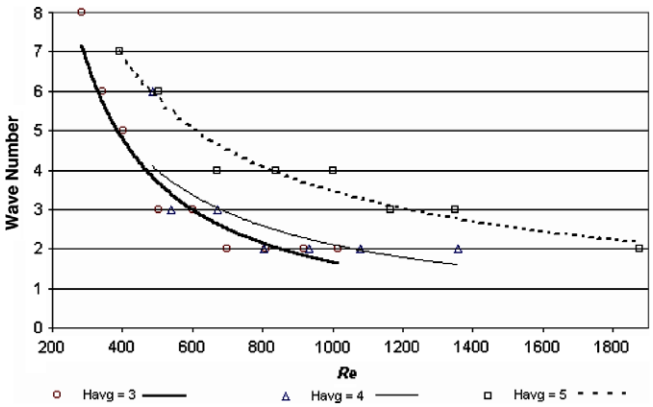

Fig. 10. Position of the first wave that presents rolling vortices (counted from the channel inlet). Model A, plane A.

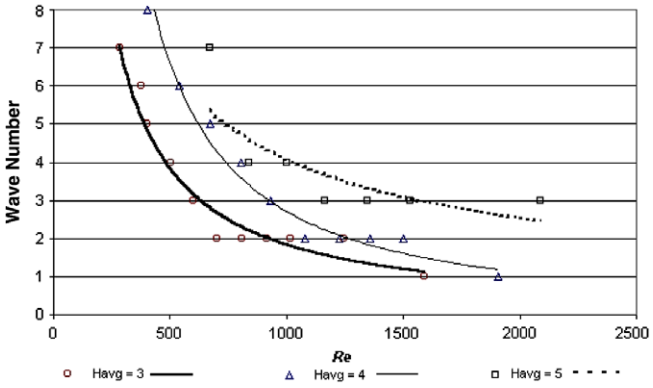

Fig. 11. Position of the first wave that presents rolling vortices (counted from the channel inlet). Model A, plane B.

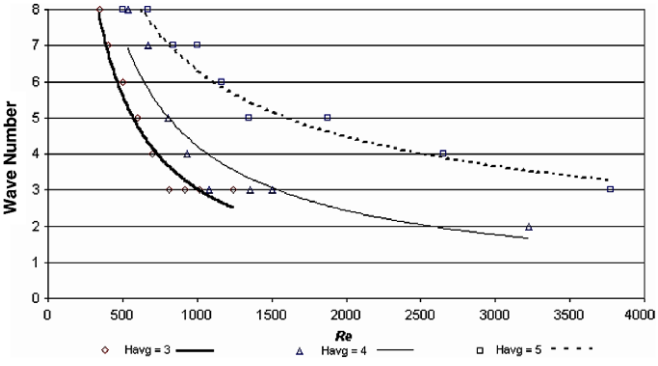

Fig. 12. Position of the first wave that presents macroscopic mixing (counted from the channel inlet). Model A, plane A.

Fig. 10 shows that an increase of the average separation between plates promotes rolling vortices to appear at larger Reynolds numbers. For example, when H_{avg} = 3 cm and Re = 500, there are already rolling vortices in wave 3, but when H_{avg} = 5 cm and Re = 840 rolling vortices first appear in wave 4. This indicates that increasing the average separation between plates makes the flow pattern in the channel steadier. As shown in Fig. 11, a similar behavior can be observed in plane B.

Decreasing the average separation between plates promotes macroscopic mixing to appear at lower Reynolds numbers (see Figs. 12 and 13); this trend is similar to that observed for rolling vortices. Increasing H_{avg} makes it more difficult for macroscopic

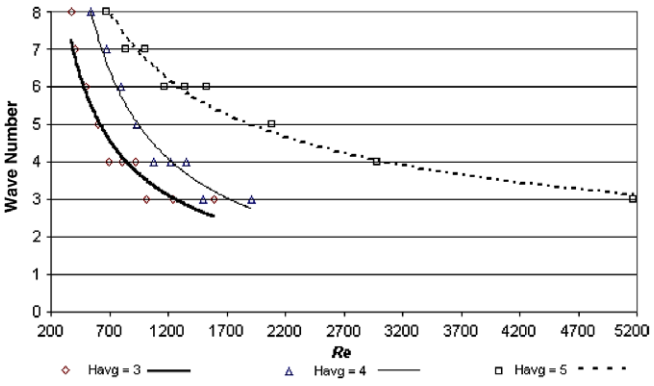

Fig. 13. Position of the first wave that presents macroscopic mixing (counted from the channel inlet). Model A, plane B.

mixing to appear at a given Reynolds number; this trend is obvious because the Reynolds number definition is based on the average separation between plates. Therefore it cannot be concluded that the channel separation is necessarily fully responsible form the change of the flow pattern.

3.2. Model B: 0° phase angle

As in model A, the average separation between plates was varied from 3 to 5 cm. The Reynolds number was varied in the laminar regime. Lower and upper Reynolds number limits were established in the same way as in model A.

The observed flow patterns in Model B were similar to those reported by Rush et al. (1999) and Zhang et al. (2004). At very low velocities ($Re \sim 200$), unlike model A, recirculation regions were not observed throughout the corrugated channel. In general, the flow moves and tries to follow the channel shape. This case is a typical Stokes flow since the viscous forces dominate the flow pattern. Steady recirculation regions could be observed in the first wave for Reynolds larger than 200. More recirculation regions are observed along the channel as the Reynolds number increases; eventually, recirculation regions and rolling vortices appear throughout the entire channel.

Figs. 14 and 15 show the flow pattern that appears in this type of channel. The results are different from those of model A; the recirculation regions in model B do not cover the entire wave. As the Reynolds number and the wavelength from the channel inlet increases, the recirculation regions increase in size and begin to cover a larger region of the channel. At large Reynolds numbers, a weak recirculation region appears in wave 1, as well as instabilities with similar characteristics to those present in model A. When the Reynolds number is increased the separation point moves closer to the beginning of the wave, and the reattachment point is closer to the end of the wave. In this case, there are not symmetric recirculation regions; this can also be observed in Figs. 14 and 15.

As the Reynolds number increases, instabilities appear in waves closer to the channel inlet. At large Reynolds numbers ($Re \sim 800$), some waves present random particle paths that promote macroscopic mixing over all the separation between plates (see Fig. 14, wave 4). It was observed that the wave number from inlet where macroscopic mixing first occurs, decreases as the Reynolds number increases. Macroscopic mixing was rarely observed in wave 1, even at very large Reynolds numbers. For large H_{avg}, it becomes difficult for macroscopic mixing to appear even in waves relatively far from the wave inlet.

Model A presents rolling vortices that appear in the limits between the principal flow and the upper part of the recirculation region, and the same behavior occurs for model B. The vortices

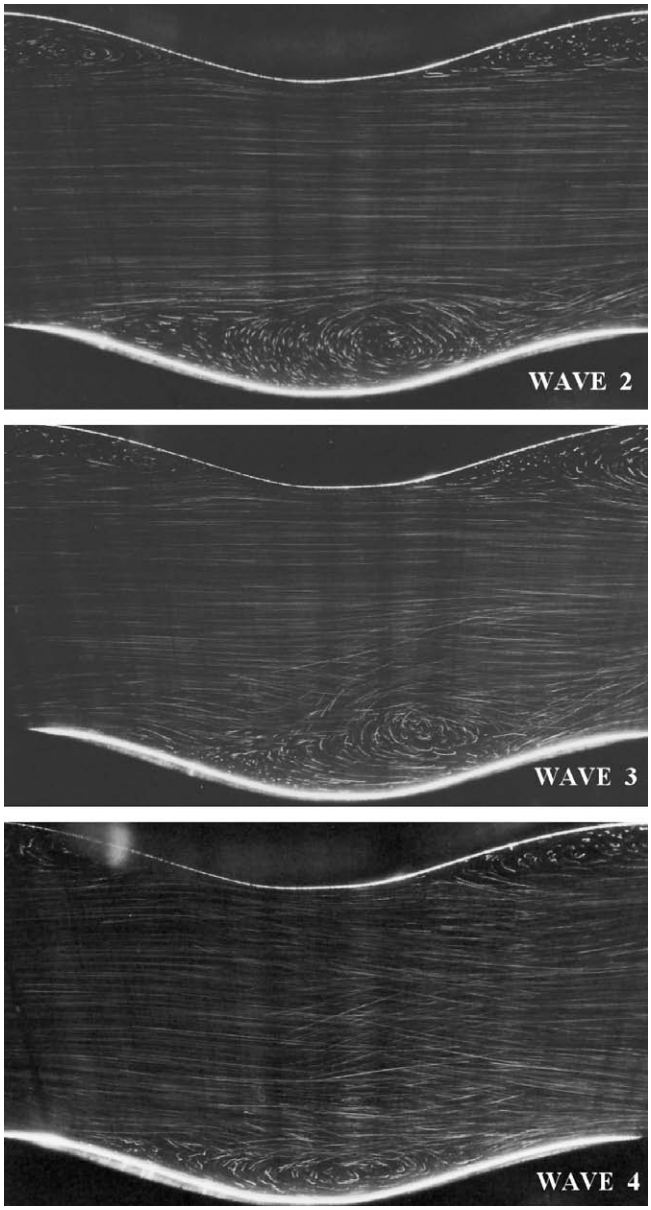

Fig. 14. Pathlines in plane A, model B. H_{avg} = 4.0 cm, Re = 800.

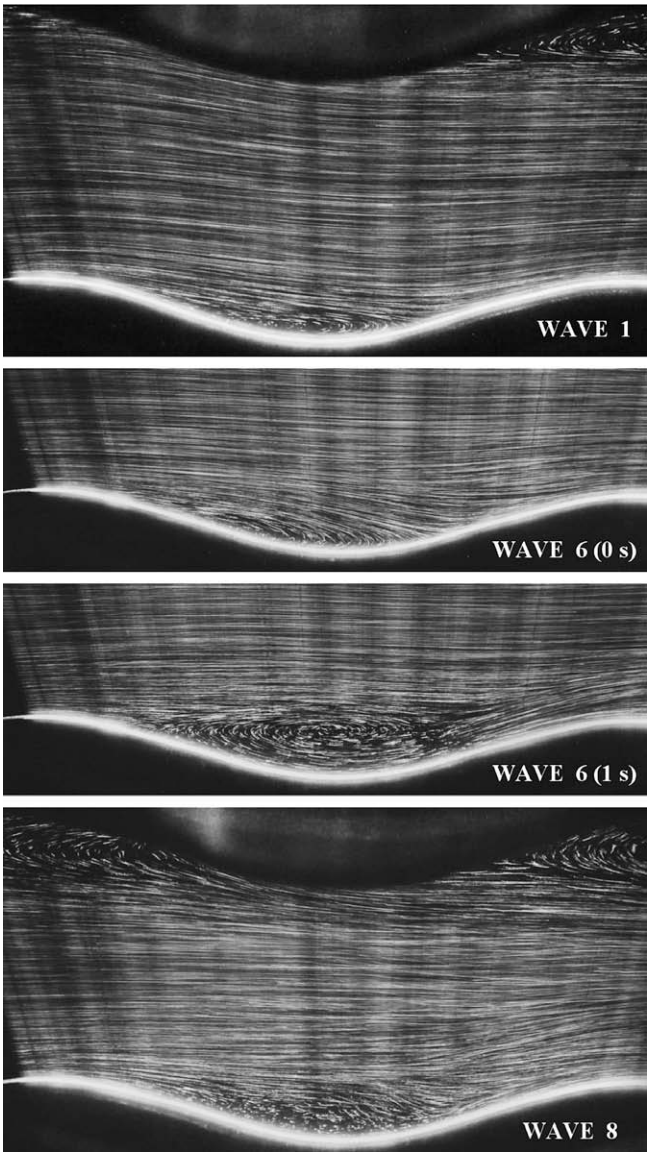

Fig. 15. Pathlines in plane B, model B. H_{avg} = 4.0 cm, Re = 400.

appear at the beginning of the wave and move downstream to the end of the wave, where they join the main core flow. If rolling vortices appear in some wave, waves with rolling vortices or macroscopic mixing are always seen downstream. When there are waves in the channel with macroscopic mixing, there are always waves with rolling vortices upstream from this wave. However, it is not necessarily true that macroscopic mixing exist when rolling vortices exist. It is believed that, for model B, instabilities in the central flow (macroscopic mixing) are created by rolling vortices and flow asymmetry. Finally, it is important to mention that rolling vortices and macroscopic mixing move closer to the channel inlet as the Reynolds number increases. One of these rolling vortices can be seen in Fig. 14, wave 2, while macroscopic mixing, manifested by instabilities in the central flow, can be clearly seen in wave 4 of the same figure. In Fig. 15, the position of a rolling vortex located in wave 6 is seen at two different instants.

Whenever macroscopic mixing appears in some wave, there are waves downstream with rolling vortices. This behavior of model B is similar to that of model A; in addition to this behavior, it can be inferred that rolling vortices instabilities appear at lower Reynolds numbers than macroscopic mixing instabilities. This behavior is independent of H_{avg} and is very similar in both planes A and B. See Figs. 16 and 17.

Figs. 18 and 19 show, for a range of the Re number, the closest wave number from the inlet, in which rolling vortices appears. The closest wave number from the inlet that presents macroscopic mixing can be observed in Figs. 20 and 21, as function of the Re number.

The graph in Fig. 18 shows that the increase of the average separation between plates promotes rolling vortices to appear at larger Reynolds numbers (the same behavior observed in model A). For example, with H_{avg} = 5 cm and Re = 840, there is already a rolling vortex in wave 4, but there is a rolling vortex in wave 2 for Re = 800 and H_{avg} = 4 cm. This indicates that increasing the average separation between plates makes the flow pattern in the channel steadier. A very similar behavior can be observed in plane B. See Fig. 19.

Decreasing the average separation between plates promotes macroscopic mixing to appear at lower Reynolds numbers; this behavior is similar to that of rolling vortices. Fig. 20 shows that wave 6 presents macroscopic mixing up to Re = 840 and H_{avg} = 5.0 cm, while wave 4 at H_{avg} = 4.0 cm already has macro-

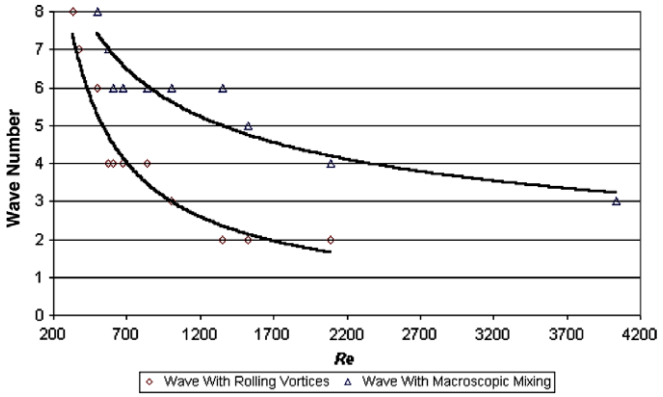

Fig. 16. Comparison between the position of the first wave that presents rolling vortices and the position of the first wave that presents macroscopic mixing. Model B, plane A, H_{avg} = 5.0 cm.

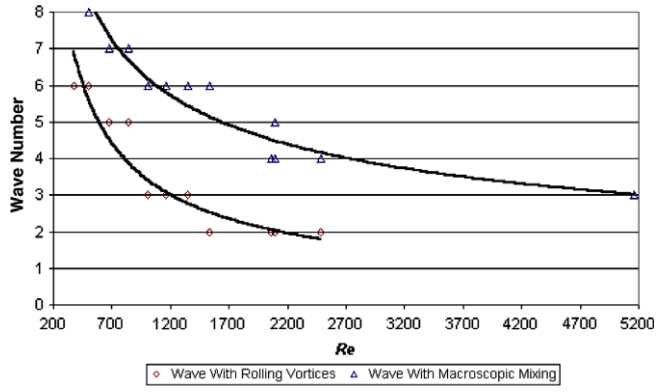

Fig. 17. Comparison between the position of the first wave that presents rolling vortices and the position of the first wave that presents macroscopic mixing. Model B, plane B, H_{avg} = 5.0 cm.

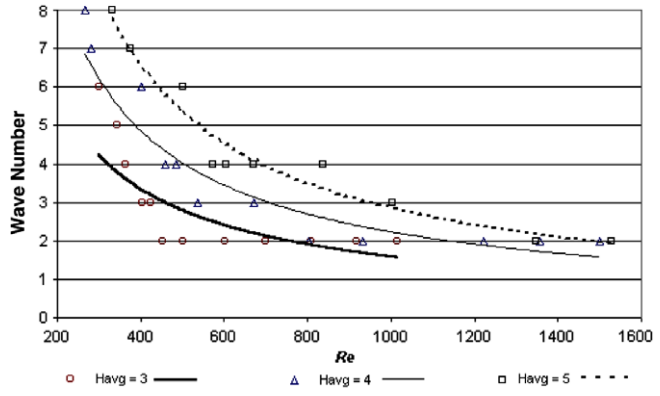

Fig. 18. Position of the first wave that presents rolling vortices (counted from the channel inlet). Model B, plane A.

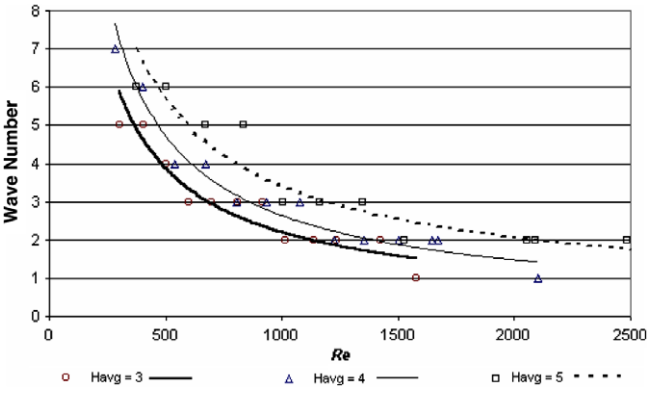

Fig. 19. Position of the first wave that presents rolling vortices (counted from the channel inlet). Model B, plane B.

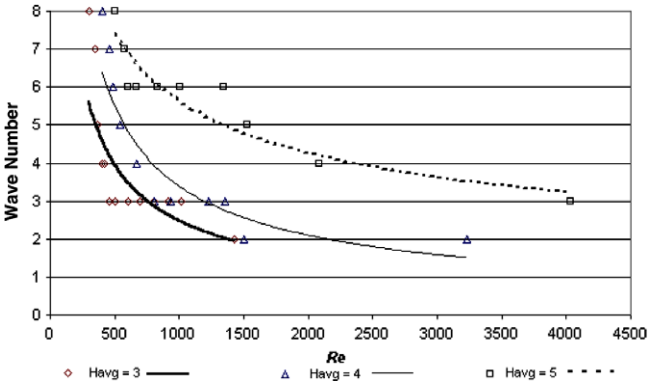

Fig. 20. Position of the first wave that presents macroscopic mixing (counted from the channel inlet). Model B, plane A.

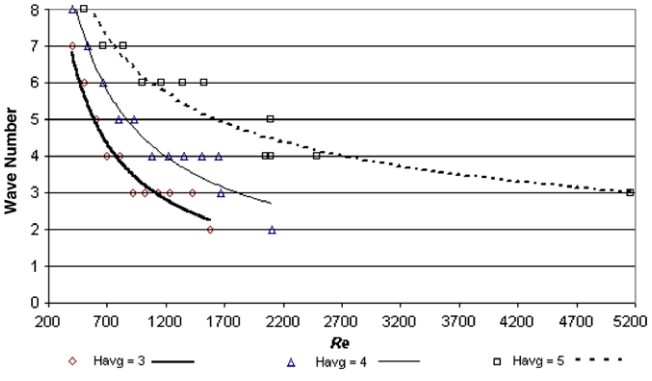

Fig. 21. Position of the first wave that presents macroscopic mixing (counted from the channel inlet). Model B, plane B.

scopic mixing at a lower Reynolds number (Re = 800). This proves that increasing H_{avg} makes more difficult for the macroscopic mixing to appear; this behavior is similar to that present in model A.

The flow pattern in this model is similar in both planes. Figs. 15, 17, 19 and 21 show the conditions for appearance of the different flow feature in plane B.

3.3. Model 1: convergent plates

Two convergence angles were considered in this investigation. The lower limit was chosen as the angle $\alpha \approx 1.37°$, in which chaotic advection with broken recirculation regions appears; the upper limit was chosen as the angle $\alpha \approx 2.6°$, in which only chaotic paths (without recirculation regions) are present.

The steady recirculation regions that occur in this model are as described before. Instabilities, such as rolling vortices and macroscopic mixing, were reduced by the convergent characteristics of this model. Rolling vortices appear at larger Reynolds numbers than those of models A and B, and macroscopic mixing does not appear for the Reynolds number range used in the present investigation. The flow in this model is affected by the stabilizing effect that the convergent channel produces over the flow.

Fig. 22 shows the flow characteristics that appear for $\alpha = 1.37°$ and $Re = 500$. In wave 1 the recirculation regions are steady. The last three photographs of Fig. 22 show the flow in wave 8 at three different times, illustrating the way rolling vortices behave. The second photograph of Fig. 23 shows that there is no symmetry of rolling vortices occurring over each plate of the channel.

The graph in Fig. 24 shows the closest wave number from inlet that presents rolling vortices. It can be observed that increasing the convergence angle makes the flow steady in a shorter interval. For example, with $\alpha = 1.37°$ and $Re = 500$, there are rolling vortices up to wave 8, whereas with $\alpha = 2.6°$, there are already rolling vortices in wave 4 for the same Reynolds number.

Fig. 25 clearly shows that the flow pattern for plane B is similar to that of plane A. For example, with $\alpha = 1.37°$ and $Re = 500$, there are rolling vortices in wave 7, while there are already vortices in wave 4 for $\alpha = 2.6°$ and $Re = 500$.

3.4. Model 2: divergent plates

The experiments for this model were also carried out in the laminar regime. Channels with divergence angles of 1.37° and 2.6° were analyzed.

Steady recirculation regions are restricted to very low Reynolds numbers, and to waves near the inlet of the channel. As opposed to model 1, rolling vortices are not very clear, and appear only in waves very close to the inlet. On the other hand, macroscopic mixing also appears in waves close to the channel inlet. This behavior is attributed to the divergent position of the plates.

Fig. 26 shows the different flow patterns that are present along the channel. The flow in waves 1 and 2 has steady recirculation regions that are symmetric with respect to the midplane of the channel. Wave 3 shows the appearance of certain asymmetry of the flow with oscillations in the size of the recirculation regions on each cavity of the channel, but without disappearance of the recirculation regions by interactions with the main flow. Wave 4 has macroscopic mixing because the recirculation regions on each cavity of the channel are broken periodically by the main core flow.

As Sawyers et al. (1998) showed, chaotic advection can be produced in steady recirculation regions by varying the flow angle. Although the flow angle is zero in this research, the divergent characteristics of this model could promote chaotic advection in steady recirculation regions. According to this, the wave that could present modified recirculation regions by chaotic advection is wave one, because it is steady in a wide range of the Reynolds number for models A and B.

Information about the presence of chaotic advection in wave 1 was not found. Sometimes, particles that crossed the visualization

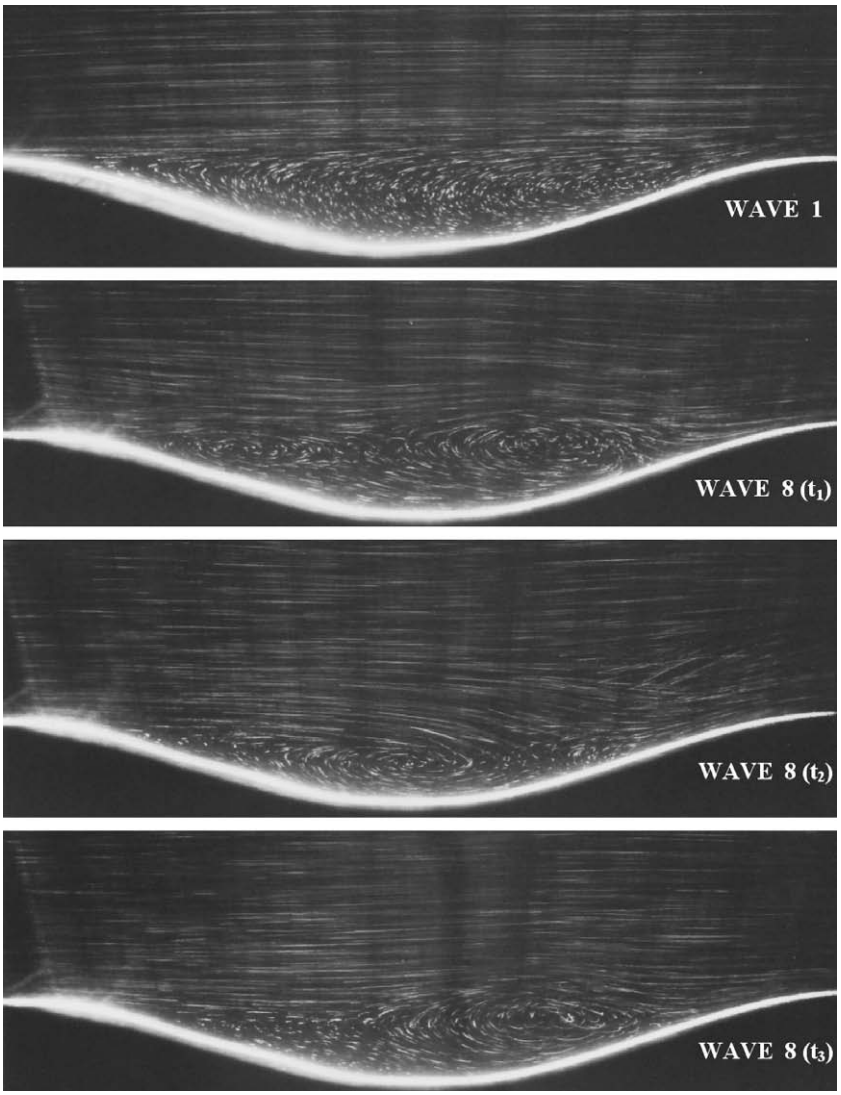

Fig. 22. Pathlines in the plane A, model 1. $\alpha = 1.37°$, $Re = 500$.

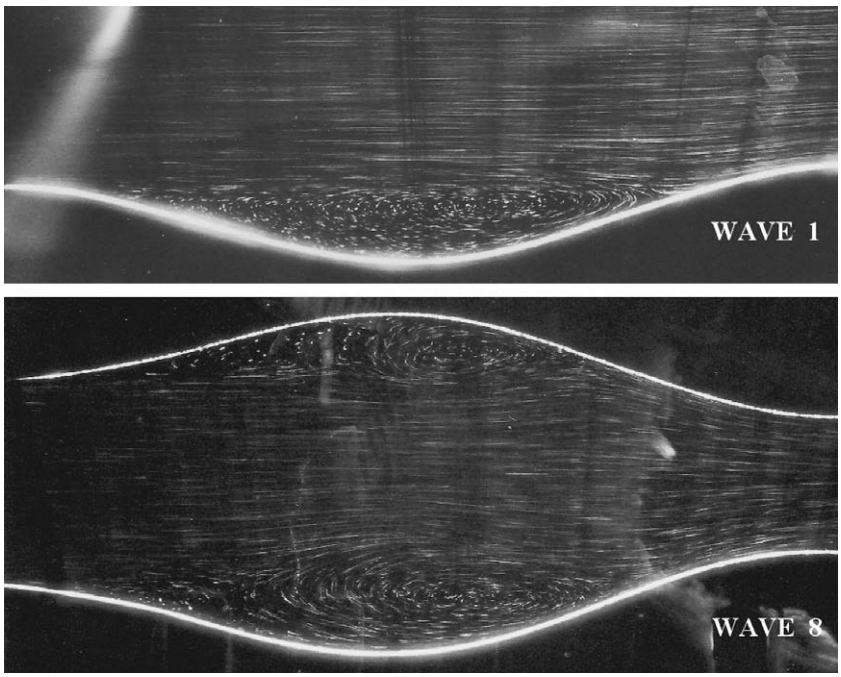

Fig. 23. Pathlines in plane B, model 1. $\alpha = 2°$, $Re = 500$.

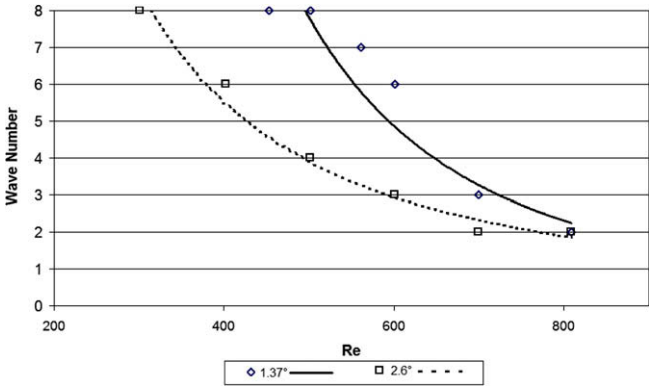

Fig. 24. First wave number from inlet with rolling vortices. Model 1, plane A.

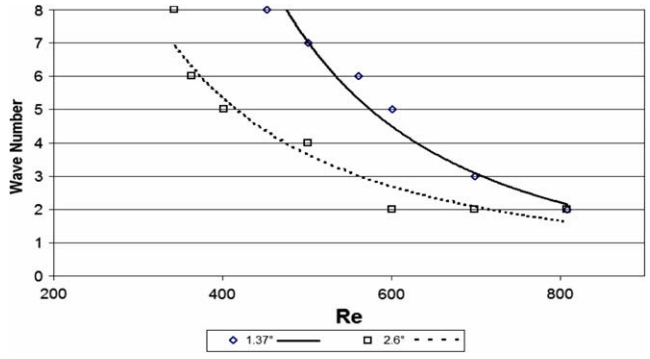

Fig. 25. First wave number from inlet with rolling vortices. Model 1, plane B.

plane were observed, but the presence of chaotic advection could not be clearly established.

According to these results, it can be stated that this model presents unsteady characteristics at the lowest Reynolds number range. This will be evidenced in the graphs shown later. Steady recirculation regions and rolling vortices appear in waves downstream from the first wave, but only for the case of small Reynolds numbers. On the other hand, increasing the divergence angle makes the flow behavior steady only for small Reynolds numbers. Rolling vortices were detected only in wave 2.

Fig. 27 shows that for a given Reynolds number macroscopic mixing appears sooner when the divergence angle is increased. For example, with $\alpha = 2.6°$ and $Re = 300$, there is macroscopic mixing from wave 4, while there is macroscopic mixing from wave 4 for $\alpha = 2.6°$ and $Re = 300$.

Fig. 28 compares the flow characteristics of model 2, with those of models A and B. Models A and B are corrugated plates of egg carton configuration with 0° and 180° phase angles, respectively, but without divergence. Flow characteristics are compared only for $H_{avg} = 3$ cm, because model 2 has $H_{avg} = 3$ cm in the first wave.

Fig. 28 shows that divergent channels are effective in promoting macroscopic mixing in corrugated plates channels, this is due to the fact that macroscopic mixing appears, at relatively small Reynolds numbers. Interestingly, macroscopic mixing does not appear for the convergent channels, unless the Reynolds number is quite large.

4. Conclusions

The visualized flow pattern for a 180° phase angle channel (model A) agrees qualitatively with the steady flow pattern found by Sawyers et al. (1998) in their numerical–analytical research related to corrugated plates with the egg carton configuration. The flow pattern in egg carton plates is very similar to the flow pattern that was found experimentally by Rush et al. (1999) and by Oviedo-Tolentino et al. (in press-a,b) in sinusoidal plates. If the characteristics observed in the steady recirculation regions of this research are compared to the analytical/numerical results obtained by Wang and Chen (2002) for sinusoidal plates, it can be said that there are similarities between both investigations.

The results obtained for model B (0° phase angle) could not be compared to other investigations, because no analogous investigation could be found in the technical literature. However, the flow

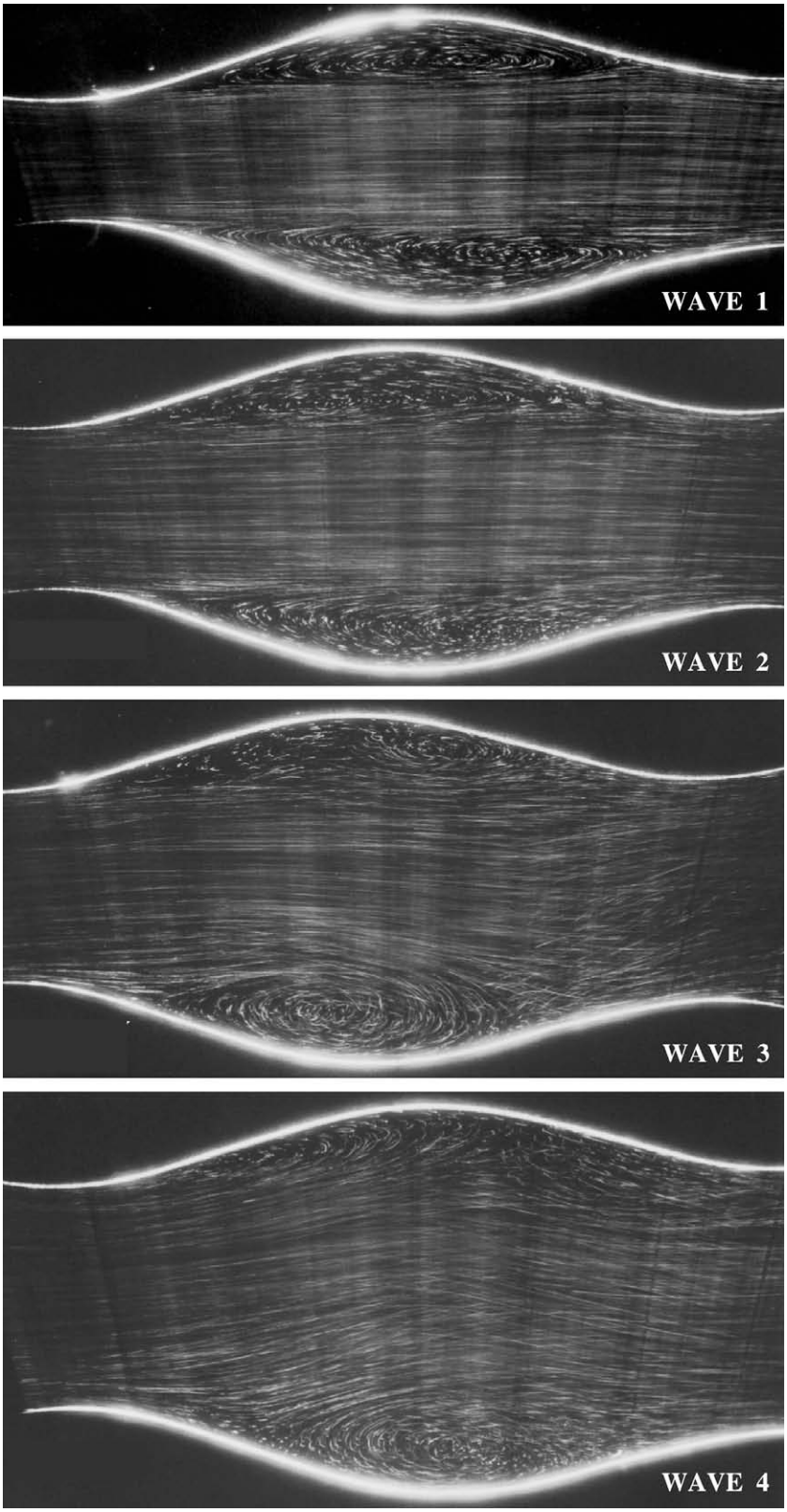

Fig. 26. Pathlines in the plane B, model 2. $\alpha = 1.37°$, $Re = 300$.

pattern found has some characteristics that are similar to the flow pattern that was found by some investigations in sinusoidal plates with 0° (Gschwind et al., 1995; Rush et al., 1999; Sawyers et al., 1998; Zhang et al., 2004). Rush et al. (1999) did not report finding rolling vortices in sinusoidal corrugated plates with 0° phase angle, while this research found them in corrugated plates with the egg carton configuration and a 0° phase angle. It is believed that the rolling vortices appearing in model B might be caused by the three-dimensionality in the egg carton configuration. However, the steady recirculation behavior is very similar to the one obtained in some numerical studies of the flow in sinusoidal corrugated plates with 0° phase angle (as the vortex pattern repeats at

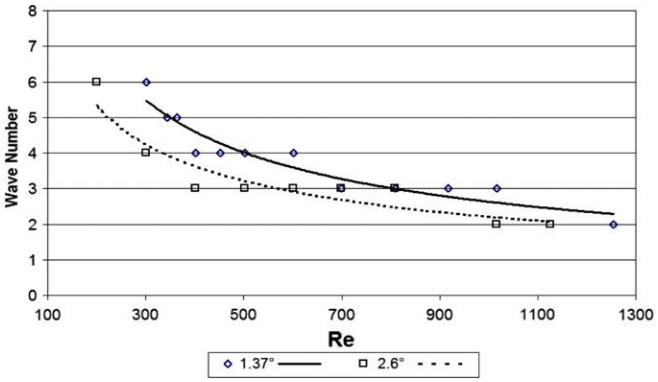

Fig. 27. First wave number from inlet with macroscopic mixing. Model 2, plane A.

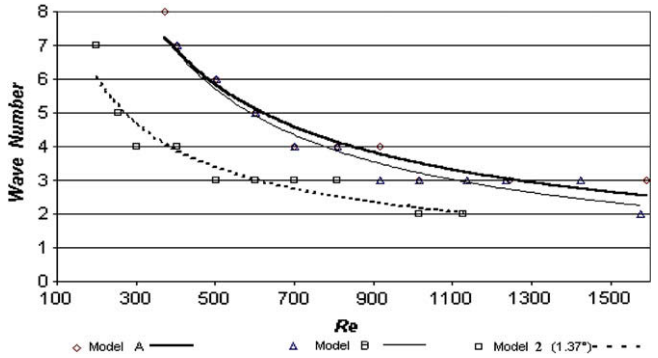

Fig. 28. First wave number from inlet with macroscopic mixing for plane B.

each wave, both in shape and position). The macroscopic mixing behavior found agrees with the results of Rush et al. (1999), because the core current interacts with each of the recirculation vortices, exchanging fluid with them periodically.

By comparing models A and B, it could be inferred that a 0° phase angle causes flow instabilities to appear at smaller Reynolds numbers than the 180° phase angle. The reason for that is related to the flow asymmetry in model B (0° phase angle). When the average separation between plates increases, it is more difficult for instabilities, like rolling vortices and macroscopic mixing, to appear; interestingly, this behavior is independent of the phase angle.

According to the technical literature, it was believed that broken recirculation regions would be seen in wave 1 for convergent or divergent plates channels, however the experiment showed that steady recirculation regions were not broken by chaotic advection. Chaotic advection was searched in wave 1 because this wave had non-broken steady recirculation regions for large Reynolds numbers for the case of parallel corrugated plates channels. Convergent and divergent plate channels are symmetric to the main core flow; this may be the reason why chaotic advection did not appear in the first wave of the channel.

According to this study, it can be concluded that divergent plates cause instabilities to appear at small Reynolds numbers; in contrast, convergent plates cause instabilities to appear at the highest-end of the Reynolds number range. Parallel corrugated plates with 0° phase angle promote instabilities to appear at smaller Reynolds numbers than parallel corrugated plates with of 180° phase angle. This behavior is caused by the flow asymmetry in corrugated plates with 0° phase angle. However, the divergent corrugated plates configuration shows the unsteadiest behavior, producing macroscopic mixing at small Reynolds numbers. The best mixing in divergent corrugated plates could imply the best temperature profile, and consequently the best heat transfer behavior.

Macroscopic mixing is an effective way to enhance the heat transfer and mixing in corrugated plates because of its random particle trajectories, and divergent plates promote this behavior in contrast to convergent plates. Although macroscopic mixing is in some way an interesting phenomena, capable of improving the heat transfer and the stirring in corrugated plates (because of its random particle advection), it does not appear in waves very near the channel inlet at the small Reynolds number range, appearing only at very large Reynolds numbers; specially for large average plates separation.

Currently, there are other investigations under way that have been able to corroborate the existence of rolling vortices and macroscopic mixing (Oviedo-Tolentino et al., in press-a,b).

Investigating the flow at other planes without flow symmetry would be helpful to understand the flow features in corrugated channel with egg carton configuration plates; these planes could have quite random particle paths at low Reynolds numbers. Planes with asymmetric flow may establish the difference between sinusoidal plates channels behavior and corrugated plates with the egg carton configuration channels. Visualization of the flow in these planes will permit gaining insight on the chaotic mixing nature of the flow. Furthermore, it is very important to perform additional experimental investigations about the existence of chaotic advection in divergent corrugated plates with the egg carton configuration. Proving that chaotic advection exist in divergent corrugated plates with the egg carton configuration will set these corrugated plates as one of the best options to improve the heat transfer in plate heat exchangers.

Some previous investigations have concluded that improving mixing and generating recirculation zones increases the heat transfer (Chagny et al., 2000; Gschwind et al., 1995; Islamoglu and Parmaksizoglu, 2004; Jones, 1994; Lefevre et al., 2003; Lemenand and Peerhossaini, 2002; Mokrani et al., 1997; Rush et al., 1999; Zhang et al., 2004). This paper presents a study in relation to the flow pattern in corrugated plates with the egg carton configuration. Additional research on the heat transfer for this corrugated plates configurations must be developed in order to prove that heat transfer is increased by recirculations, rolling vortices, and random particle paths. Up to date there are no numerical simulations able to accurately reproduce the flow features observed in this and other experimental investigations; for these reason, experimental studies regarding heat transfer in chaotic mixing channels are needed to provide the information that relates chaotic mixing promotion to heat transfer enhancement.

Acknowledgments

The authors would like to acknowledge the support of the Mexican Council for Science and Technology (CONACyT) under Grant J-37328-U. Special credit is given to Mr. Mauro Azúa and Mr. Manuel Lozano for their help and advice during the planning of the experiments.

References

Braun, H., Neumann, H., Mitra, N.K., 1999. Experimental and numerical investigation of turbulent heat transfer in a channel with periodically arranged rib roughness elements. Experimental Thermal and Fluid Science (19), 67–76.

Chagny, C., Castelain, C., Peerhossaini, H., 2000. Chaotic heat transfer for heat exchanger design and comparison with a regular regime for a large range of Reynolds numbers. Applied Thermal Engineering 20, 1615–1648.

Chang, H.C., Sen, M., 1994. Application of chaotic advection to heat transfer. Chaos, Solitons & Fractals 4, 955–975.

DeJong, N.C., Jacobi, A.M., 2003. Flow, heat transfer, and pressure drop in the near wall region of louvered-fin arrays. Experimental Thermal and Fluid Science 27, 237–250.

El-Sayed, S.A., Mohamed, S.M., Abdel-latif, A.M., Abouda, A.H.E., 2002. Investigation of turbulent heat transfer and fluid flow in longitudinal rectangular-fin arrays of

different geometries and shrouded fin array. Experimental Thermal and Fluid Science 26, 879–900.
Froncioni, A.M., Muzzio, F.J., Peskin, R.L., Swanson, P.W., 1997. Chaotic motion of fluid and solid particles in plane wakes. Chaos, Solitons & Fractals 8, 109–130.
Galaktionov, O.S., Anderson, P.D., Peters, G.W.M., Tucker III, C.L., 2002. A global, multi-scale simulation of laminar fluid mixing: the extended mapping method. International Journal of Multiphase Flow 28, 497–523.
Gschwind, P., Regele, A., Kottke, V., 1995. Sinusoidal wavy channels with Taylor–Goertler vortices. Experimental Thermal and Fluid Science 11, 270–275.
Herman, C., Kang, E., 2002. Heat transfer enhancement in a grooved channel with curved vanes. International Journal of Heat and Mass Transfer 45, 3741–3757.
Howes, T., Shardlow, P.J., 1997. Simulation of mixing in unsteady flow through a periodically obstructed channel. Chemical Engineering Science 52, 1215–1225.
Islamoglu, Y., Parmaksizoglu, C., 2004. Numerical investigation of convective heat transfer and pressure drop in a corrugated heat exchanger channel. Applied Thermal Engineering 24, 141–147.
Jang, J.Y., Chen, L.K., 1997. Numerical analysis of heat transfer and fluid flow in a three-dimensional wavy-Fin and tube heat exchanger. International Journal of Heat and Mass Transfer 40, 3981–3990.
Jones, S.W., 1994. Interaction of chaotic advection and diffusion. Chaos, Solitons & Fractals 4, 929–940.
Lefevre, A., Mota, J.P.B., Rodrigo, A.J.S., Saatdjian, E., 2003. Chaotic advection and heat transfer enhancement in Stokes flows. Experimental Thermal and Fluid Science 24, 310–321.
Lemenand, T., Peerhossaini, H., 2002. A thermal model for prediction of the Nusselt number in a pipe with chaotic flow. Applied Thermal Engineering 22, 1717–1730.
Lin, C., Chiu, P.H., Shieh, S.J., 2002. Characteristics of horseshoe vortex system near a vertical plate-base plate juncture. Experimental Thermal and Fluid Science 27, 25–46.
Liu, M., Muzzio, F.J., Peskin, R.L., 1994. Quantification of mixing in aperiodic chaotic flows. Chaos, Solitons & Fractals 4, 869–893.
Lyman, A.C., Stephan, R.A., Thole, K.A., Zhang, L.W., Memory, S.B., 2002. Scaling of heat transfer coefficients along louvered fins. Experimental Thermal and Fluid Science 26, 547–563.
Mahmud, S., Sadrul-Islam, A.K.M., Mamun, M.A.H., 2002. Separation characteristics of fluid flow inside two parallel plates with wavy surface. International Journal of Engineering Science 40, 1495–1509.
Mokrani, A., Castelain, C., Peerhossaini, H., 1997. The effects of chaotic advection on heat transfer. International Journal of Heat and Mass Transfer 40, 3089–3104.
Nishimura, T., Kawamura, Y., 1995. Three-dimensionality of oscillatory flow in a two-dimensional symmetric sinusoidal wavy-walled channel. Experimental Thermal and Fluid Science 10, 62–73.
Oviedo-Tolentino, F., Romero-Méndez, R., Hernández-Guerrero, A., Girón-Palomares, B., in press-a. Use of diverging or converging sinusoidal plate channels for the control of chaotic mixing in plate heat exchangers. Experimental Thermal and Fluid Science.
Oviedo-Tolentino, F., Hernández-Guerrero, A., Romero-Méndez, R., Girón-Palomares, B., in press-b. Experimental study in the progress of fluid flow in a sinusoidal channel. Experiments in fluids.
Raynal, F., Gence, J.N., 1997. Energy saving in chaotic laminar mixing. International Journal of Heat and Mass Transfer 40, 3267–3273.
Romero-Méndez, R., Sen, M., Yang, K.T., McClain, R., 2000. Effect of fin spacing on convection in a plate fin and tube heat exchanger. International Journal of Heat and Mass Transfer 43, 39–51.
Rush, T.A., Newell, T.A., Jacobi, A.M., 1999. An experimental study of flow and heat transfer in sinusoidal wavy passages. International Journal of Heat and Mass Transfer 42, 1541–1553.
Sawyers, R., Sen, M., Hsueh-Chia, C., 1998. An experimental study of flow and heat transfer in sinusoidal wavy passages. International Journal of Heat and Mass Transfer 41, 3559–3573.
Southerland, K.B., Frederiksen, R.D., Dahm, W.J.A., Dowling, D.R., 1994. Comparisons of mixing in chaotic and turbulent flows. Chaos, Solitons & Fractals 4, 1057–1089.
Stone, K., Vanka, S.P., 1999. Numerical study of developing flow and heat transfer in a wavy passage. Journal of Fluids Engineering 121, 713–719.
Tabor, M., Klapper, I., 1994. Stretching and alignment in chaotic and turbulent flows. Chaos, Solitons & Fractals 4, 1031–1055.
Wang, C.C., Chen, C.K., 2002. Forced convection in a wavy-walled channel. International Journal of Heat and Mass Transfer 45, 2587–2595.
Zhang, J., Kundu, J., Manglik, R.M., 2004. Effect of fin waviness and spacing on the lateral vortex structure and laminar heat transfer in wavy-plate-fin cores. International Journal of Heat and Mass Transfer 47, 1719–1730.